Chemical Physics 175 (1993) 113–125
North-Holland

State-to-state vibrational energy transfer in acetylene gas, measured by fluorescence-detected Raman–ultraviolet double resonance spectroscopy

B.L. Chadwick, A.P. Milce and B.J. Orr [1]
School of Chemistry, Macquarie University, NSW 2109, Australia

Received 25 February 1993

Fluorescence-detected Raman–ultraviolet double resonance spectroscopy enables state-selective investigations of vibrational energy transfer in gas-phase acetylene, C_2H_2. Pulsed coherent Raman excitation of the $(\nu_2+\nu_4-\nu_4)$ rovibrational hot band of $C_2H_2(g)$ is followed by rovibronic probing of collision-induced population transfer to the ν_2 vibrational level. This time-resolved spectroscopic technique provides novel kinetic and mechanistic information on the quasi-elastic intermolecular V–V transfer process: $C_2H_2(\nu_2+\nu_4)+C_2H_2(v=0)\rightarrow C_2H_2(\nu_2)+C_2H_2(\nu_4)$. The state-to-state second-order rate constant for this process is measured and its relevance to the dynamics of vibrational energy transfer is discussed. The results demonstrate the advantages of rotationally resolved double-resonance techniques in elucidating vibrational energy transfer processes.

1. Introduction

This paper is concerned with collision-induced, state-to-state vibrational energy transfer within the ground electronic manifold of gas-phase acetylene molecules. There is an extensive body of literature on this subject for various small polyatomic molecules, represented by a selection of relevant books and reviews [1–4]. Our interest concentrates on the technique of time-resolved optical double resonance (ODR) spectroscopy [5], the versatility and sensitivity of which has long been recognised in the context of vibrational energy transfer. Other state-specific techniques such as infrared fluorescence (IRF) [6] have proved useful in yielding collisional efficiencies $\mathscr{P}$ for V–V and V–T, R processes in many molecules [#1] but these are usually resolved only at the level of individual vibrational states. ODR techniques have the potential to provide more detailed, rotationally resolved information on vibrational energy transfer.

The ODR approach employs one laser pulse to prepare an initial rovibrational population, and a second laser (either cw or pulsed) to probe the subsequent growth and decay of population, both in the initially prepared state and in other states populated by the energy transfer processes of interest. Such a technique is able to select and probe individual rotational states of a vibrational manifold, but is does not necessarily convey any more information on V–V transfer than lower-resolution techniques such as IRF. This is because accompanying collision-induced rotational energy transfer (RET) usually "scrambles" the rotational state(s) prepared by infrared excitation before any discernible V–V transfer takes place. One is then measuring the vibrational relaxation of a thermally equilibrated array of rotational states and likely only to derive rotationally averaged V–V transfer rates. Nevertheless, ODR techniques are often advantageous, relative to lower-resolution methods such as IRF, because of their high sensitivity, state-specificity and amenability to fast detection-system response.

There are some instances where the ODR spectra of a rotationally relaxed system undergoing V–V transfer may exhibit clear rotational (or other angular-momentum-related) propensities in the energy

[1] To whom correspondence should be addressed.

[#1] It is customary to define the collisional efficiency $\mathscr{P}$ as the ratio of the rate constant (or cross section) for the process of interest to that for a reference process, such as either hard-sphere or Lennard-Jones collisions [7].

transfer channels. Instances of this are provided by infrared–infrared double resonance studies of a variety of small polyatomic molecules, by Doyennette et al. [8] and by Steinfeld et al. [9]. Moreover, it is possible (even if rare) to find specific situations in which the efficiencies of collision-induced RET and V–V transfer are comparable, so that rotationally specific channels of V–V transfer can be discerned. For example, this has been borne out by a remarkably efficient collision-induced V–V transfer channel between the ν_6 and ν_4 vibrational modes of formaldehyde-d_2, D_2CO:

$$D_2CO(v_6=1; J, K_a, K_c)+M \rightarrow D_2CO(v_4=1; J', K'_a, K'_c)+M, \quad (1)$$

where M is a collision partner (either another D_2CO molecular or a foreign-gas molecule) [#2]. This type of process has been characterised spectroscopically and kinetically by time-resolved infrared–ultraviolet double resonance (IR–UV DR) [10]. For self-collisions ($M=D_2CO$) [10–12], the *macroscopic* collisional efficiency $\mathscr{P}$ (referred to a D_2CO/D_2CO hard-sphere collisional rate constant of $\approx 10\ \mu s^{-1}\ Torr^{-1}$) for processes as shown in eq. (1) is found to be as high as 4, favoring the $K_a=4\rightarrow 6$ transfer channel [#3].

It has been shown [3,10,11] that this high collisional efficiency arises from a subtle combination of Coriolis and asymmetric-rotor perturbations, generating non-zero matrix elements of the permanent electric dipole moment between different rovibrational eigenstates of the state-selected molecule. This is a particularly clear example of the way in which intramolecular perturbations can influence the efficiency of V–V transfer, both with regard to overall efficiency and rotational specificity [3,4].

It is found [10,12] that $\nu_6\rightarrow\nu_4$ transfer in D_2CO/D_2CO collisions is rotationally selective, not only with respect to the prolate-rotor quantum number K_a but also to the total angular momentum quantum number J, with a $\Delta J=0$ propensity and a net *microscopic* rate constant (see footnote 3) of $\approx 2.5\ \mu s^{-1}\ Torr^{-1}$ (corresponding to a microscopic efficiency $\mathscr{P}$ of ≈ 0.25). This efficiency is less than that of accompanying RET [13], so that the observed V–V transfer occurs within a manifold which is (at least partially) rotationally scrambled. However, experiments with foreign-gas collision partners such as Ar and N_2O suggest [10,12,14] that judicious choice of foreign-gas collision partner ($M\neq D_2CO$) can narrow the gap between the rates of V–V transfer and rotational relaxation and make rotational specificity in rovibrational energy transfer more directly observable.

The present paper is primarily concerned with rotationally resolved experiments on V–V transfer in acetylene, C_2H_2, using fluorescence-detected Raman–ultraviolet double resonance (Raman–UV DR) spectroscopy. This time-resolved technique, as illustrated in fig. 1, comprises state-specific rovibrational excitation by two-color coherent Raman irradiation with PUMP and STOKES pulses, followed by rovibronic excitation by a UV PROBE pulse and detection of laser-induced fluorescence (LIF). The PROBE can be tuned *either* to coincide with a transition from the initially prepared rovibrational state *or* to monitor other states populated by state-to-state energy transfer, as a function of PUMP–PROBE time delay t. Information on energy-transfer kinetics and mechanisms, as well as spectroscopy, is thereby obtained. The Raman–UV DR excitation scheme depicted in fig. 1 is devised to monitor quasi-resonant intermolecular V–V transfer, in which two colliding C_2H_2 molecules exchange a quantum of the CCH trans-bending mode (ν_4), as will be explained in sections 2 and 3.

Acetylene is amenable to investigation by LIF-detected ODR, using either Raman–UV DR [15–19] or various forms of IR–UV DR [16,20–28]. This yields rotationally resolved spectroscopic and kinetic information at various levels of vibrational excitation, from the fundamental range ($\leqslant 3500\ cm^{-1}$) to the congested region of high overtone and combination levels (up to $13000\ cm^{-1}$, extendible by stimu-

[#2] Rotational quantum numbers of form (J, K_a, K_c) are those for a prolate asymmetric rotor (such as D_2CO). Primes denote the (identifiable) rotational state(s) populated in the course of the rotationally selective V–V transfer process. The two relevant vibrational modes of D_2CO are ν_4 ($938.0\ cm^{-1}$, species b_1) and ν_6 ($989.25\ cm^{-1}$, b_2).

[#3] *Macroscopic*, or phenomenological, rate constants are obtained empirically from curves of best fit to the collision-induced kinetics for the overall processes of interest. They should not be confused with *microscopic* state-to-state rate constants, which refer (more rigorously) to the individual mechanistic relaxation channels constituting the details of a kinetic model. The two forms of rate constant tend to differ markedly in complex kinetic situations, such as the multi-channel energy transfer processes considered here.

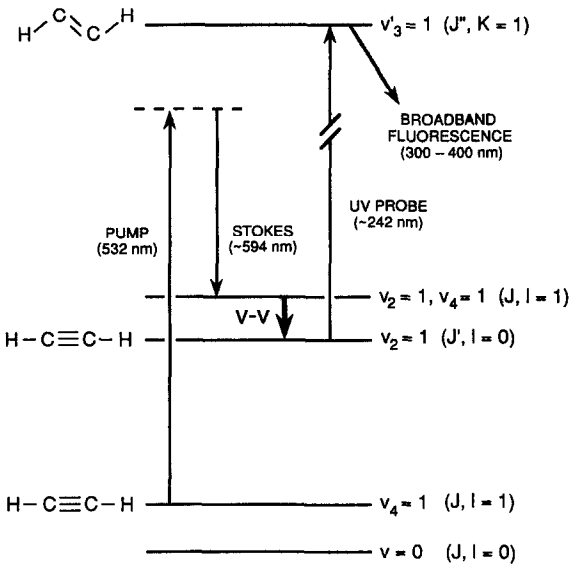

Fig. 1. LIF-detected excitation schemes for time-resolved Raman–UV DR spectroscopy of $(2_1 4_1 + 0) \rightarrow (2_1 + 4_1)$ V–V energy transfer in C_2H_2(g), as defined in eq. (1) and discussed in detail in section 2. Rovibrational excitation of the $2_1 4_1$ ($l = 1, \pi_g$) combination level is achieved by coherent Raman pumping of Q(J) transitions in the 1961.9 cm^{-1} ($\nu_2 + \nu_4 - \nu_4$) hot band. UV PROBE radiation then accesses vibronic bands in the $\tilde{A} \leftarrow \tilde{X}$ absorption system, a trans-bent←linear transition. LIF-detected probing of the 246 nm $2_1^0 3_0^1 4_1^0$ rovibronic band, with short Raman–UV delay, can be used to monitor the direct Raman excitation process (not shown explicitly in this figure). With the Raman–UV delay adjusted to enable collision-induced V–V transfer (bold arrow), growth of population in the 2_1 vibrational level can be monitored by LIF-detected Raman–UV DR probing of the 242 nm $2_1^0 3_0^1$ rovibronic band.

lated emission pumping [29] to ≈ 16000 cm^{-1}). Such double-resonance experiments on acetylene are complemented by a number of earlier studies of vibrational energy transfer, entailing IRF [30–32], ultrasonic dispersion [33], photoacoustic absorption spectroscopy (PAS) [34], and their theoretical interpretation [35,36]. From this body of research emerges an increasingly detailed view of the dynamics of intermolecular and intramolecular processes within the rotational and vibrational manifolds of acetylene.

Since acetylene is a linear, centrosymmetric molecule in its ground electronic state, its vibrational modes divide into two categories: those which are infrared-active and those which are Raman-active. Raman–UV DR and IR–UV DR experiments are therefore complementary, since each tends to access a different set of vibrational levels for the purposes of molecular spectroscopy and energy transfer. The IR–UV DR approach has on several occasions [28,32, 37,38] yielded information on state-to-state vibrational energy transfer in gas-phase acetylene. As far as we are aware, however, corresponding results have not previously been derived from Raman–UV DR experiments for any molecule, let alone acetylene.

2. Spectroscopic details and experimental strategy

LIF-detected Raman–UV DR investigations of acetylene are now well established in terms of their spectroscopic sensitivity and utility [15,18,19], and the method's applicability to rovibrational energy transfer is also apparent [16,17]. The customary Raman–UV DR approach entails coherent Raman excitation, in the ν_2 (C≡C stretch, 1974.3 cm^{-1}, σ_g^+) band of C_2H_2, thereby preparing discrete rovibrational states. The Raman-induced rovibrational population in the 2_1 ($\nu_2 = 1$) level is then monitored by exciting vibronic bands of form $2_1^0 3_0^x$ (where $x = 1$, 2, 3, ...) in the $\tilde{A}\,^1A_u \leftarrow \tilde{X}\,^1\Sigma_g^+$ electronic absorption system of C_2H_2 [39], with undispersed LIF for detection [#4]. This choice of vibronic absorption bands satisfies limitations placed on Franck–Condon factors by the change in geometry (bent←linear) of C_2H_2 upon electronic excitation [15,18]. Fig. 2 shows a Raman–UV DR difference spectrum of the $\tilde{A} \leftarrow \tilde{X}$ $2_1^0 3_0^1 K_0^1$ band of C_2H_2 at ≈ 41300 cm^{-1}, obtained with broadband (≈ 0.3 cm^{-1}) Raman excitation spanning an envelope of ν_2-band Q(J) Raman transitions (for $J = 0$–15) and with the LIF excitation wavelength scanned [15,18]. Superimposed grids indicate the rotational structure of this band, with

[#4] We employ a standard spectroscopic notation [39], which may be understood in terms of a specific example. The symbol $2_1^0 3_0^1$ denotes a vibronic band involving a transition from the 2_1 ($\nu_2 = 1$) level in the $\tilde{X}\,^1\Sigma_g^+$ ground electronic manifold to the 3^1 ($\nu'_3 = 1$) level of the $\tilde{A}\,^1A_u$ electronically excited manifold. The vibration ν'_3 is the electronically excited CCH trans-bending mode (1048 cm^{-1}, a_g). The occasionally added annotation K_0^1 (as in $2_1^0 3_0^1 K_0^1$) specifies the angular momentum quantum numbers l ($=0$) in the linear ground electronic state and K_a ($=1$) in the non-linear upper electronic state. This addition distinguishes different rovibronic subbands, particularly in cases where $l \geq 1$.

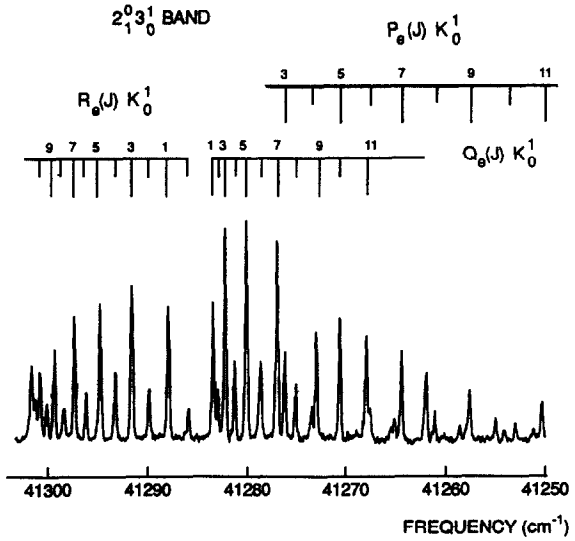

Fig. 2. LIF-detected Raman–UV DR difference spectrum of the low-J portion of the 242 nm $\tilde{A}\leftarrow\tilde{X}$ $2_1^0 3_0^1 K_0^1$ vibronic band of C_2H_2(g) at 1 Torr and 300 K, with rotational structure as indicated (see footnotes 4 and 5). The coherent Raman excitation conditions comprise: 40 mJ of 532 nm PUMP radiation; 17 mJ of 594 nm STOKES radiation; $\omega_{PUMP}-\omega_{STOKES}=1974.1$ cm^{-1}, centered on the Q(5) line of the ν_2 rovibrational band; Raman excitation bandwidth ≈ 0.3 cm^{-1}, spanning a range of Q-branch transitions. The Raman–UV delay is 10 ns, to minimise RET effects, and the LIF excitation spectrum is recorded with a UV PROBE bandwidth of 0.4 cm^{-1}.

characteristic overlapping red-degraded P and Q branches and an R branch forming a head at $J\approx 10$ [#5]. The intensity alternation with J is attributable to the ortho/para nuclear-spin statistics of the centrosymmetric C_2H_2 molecule in a state with $l=0$.

Fig. 1 shows the excitation scheme employed for our Raman–UV DR experiments on V–V transfer in C_2H_2. As a variant of Raman–UV DR schemes used previously [15–19], it enables processes of the following form to be monitored:

$$C_2H_2(2_14_1; J, l=1)+C_2H_2(v=0; \bar{J}, l=0)$$
$$\rightarrow C_2H_2(2_1; J', l=0)+C_2H_2(4_1; \bar{J}', l=1), \quad (2a)$$
$$\rightarrow C_2H_2(2_1; \bar{J}', l=0)+C_2H_2(4_1; J', l=1), \quad (2b)$$

[#5] The "subscript e" notation refers to the conventional e/f labeling of parity-doublet states in linear molecules [40]. For non-degenerate vibrational levels of acetylene, such as $2_1(\nu_2=1)$, all states are labeled "e". Levels with vibrational angular momentum quantum number $l\geq 1$ occur as a doublet, with components labeled "e" and "f", respectively.

where 2_14_1 denotes a vibrational combination level (species π_g) at 2575 cm^{-1}, comprising quanta of the ν_4 (CCH trans-bend, 612.9 cm^{-1}, π_g) and ν_2 vibrational modes. The notation $\bar{J}$ denotes the thermal-equilibrium distribution of rotational states of the collision-partner molecules, whereas the unadorned form of J denotes the specific rotational state(s) of the state-selected molecules. Without allowing for any rotational-state changes (i.e., assuming that $J=J'$, etc.), the process in eq. (2) is slightly endothermic with $\Delta E=12.5$ cm^{-1}; since $\Delta E \ll k_BT$ such a process may be regarded as quasi-elastic. For the purposes of subsequent discussion, we shall refer (in a fairly obvious form of shorthand) to the process depicted in eq. (2) as "$(2_14_1+0)\rightarrow(2_1+4_1)$" V–V transfer.

Coherent Raman excitation is achieved by the combination of two laser wavelengths (PUMP and STOKES). The PUMP wavelength is fixed at 532 nm and the STOKES wavelength is adjusted such that the Raman difference frequency ($\omega_{PUMP}-\omega_{STOKES}$) equals the frequency of the Raman-active rovibrational transition of interest. For the purposes of recording fig. 2 (and also in refs. [15,17–19]), this was the fundamental ν_2 (C≡C stretching) rovibrational band of C_2H_2. In the context of fig. 1 and eq. (2), however, the object is to excite the 2_14_1 combination level of C_2H_2. This can be achieved by Raman excitation in the 1961.9 cm^{-1} ($\nu_2+\nu_4-\nu_4$) rovibrational sequence band [41] and by LIF probing, in Raman–UV DR fashion, involving rovibronic bands of form $2_1^0 3_0^x 4_1^0$. The rovibrational excitation process entails a hot-band transition with molecules originating in the low-lying doubly degenerate 4_1 level, which has a substantial fractional population (9%, compared to 84% for the $v=0$ ground state) in C_2H_2(g) at 300 K. Moreover, this relatively small population disadvantage of ($\nu_2+\nu_4-\nu_4$)-band excitation is partially offset by an extra CCH trans-bending quantum in the 2_14_1 vibrational level, which enhances the Franck–Condon factors (and hence the detection sensitivity) for $2_1^0 3_0^x 4_1^0$ vibronic bands, relative to the $2_1^0 3_0^x$ bands used to monitor ν_2-band Raman excitation.

The 2_14_1 vibrational level is sufficiently different from the 2_1 level to be of intrinsic spectroscopic interest. It is doubly degenerate, with vibrational symmetry π_g and angular momentum quantum number $l=1$, in comparison to $l=0$ for the $2_1(\sigma_g^+)$ level. In

the $\tilde{A}\leftarrow\tilde{X}$ absorption system of C_2H_2, rovibronic bands in which the lower state has $l=1$ are composed of two principal subbands (K_1^0 and K_1^2) with $\Delta K=-1$ and $\Delta K=+1$ respectively. These two principal subbands are clearly seen in fig. 3, which is a Raman–UV DR difference spectrum of the $2_1^0 3_0^1 4_1^0$ band at ≈ 40700 cm^{-1} [18] obtained by centering the Raman excitation frequency at ≈ 1961 cm^{-1} in the Q branch of the $(\nu_2+\nu_4-\nu_4)$ hot band and scanning the UV LIF excitation wavelength. It is expected that spectra emanating from gerade vibrational levels of C_2H_2 should exhibit a 1:3 even:odd intensity alternation with J, provided that one of the states has K (or l) $=0$; this is borne out in the $2_1^0 3_0^1 4_1^0 K_1^0$ subband of fig. 3. When neither state has $K=0$, as in the $2_1^0 3_0^1 4_1^0 K_1^2$ subband of fig. 3, the successive J-rotational lines consist of a closely-spaced doublet with weak and strong components (see footnote 5), this results in a more complicated (but usually small, if not negligible) intensity alternation, as in the K_1^2 subband. Raman–UV DR spectra such as that in fig. 3 (and in the $2_1^0 3_0^2 4_1^0$ band which has also been observed at ≈ 41700 cm^{-1} [18]) contain useful spectroscopic information, since rovibronic bands of form $2_1^0 3_0^x 4_1^0$ have not previously been observed in UV absorption spectra of acetylene. The $2_1 4_1$ vibrational level has been characterised previously by rotational analysis of IR spectra of the $(\nu_2+\nu_4-\nu_5)$ hot band [42] and of high-resolution Raman spectra of the $(\nu_2+\nu_4-\nu_4)$ hot band [41].

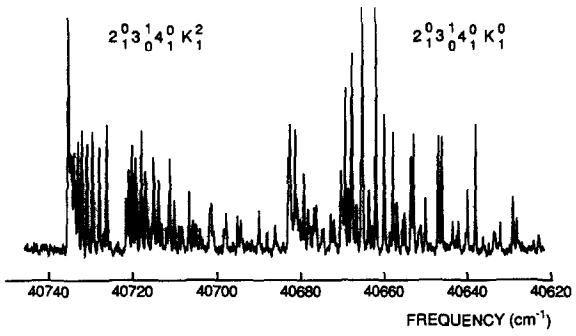

Fig. 3. LIF-detected Raman–UV DR difference spectrum of the low-J portion of the 246 nm $\tilde{A}\leftarrow\tilde{X}$ $2_1^0 3_0^1 4_1^0$ vibronic band of C_2H_2(g) at 1 Torr and 300 K, recorded with experimental conditions comparable to those of fig. 2. The Raman excitation is in the Q branch of the 1961 cm^{-1} $(\nu_2+\nu_4-\nu_4)$ rovibrational hot band. The K_1^0 and K_1^2 subbands are clearly discernible at ≈ 246 nm and ≈ 245.5 nm, respectively (see footnote 4).

The experimental conditions are similar to those employed in our previous Raman–UV DR studies of acetylene [18]. Industrial-grade C_2H_2(g) is purified by passage through an acetone/dry-ice trap and several liquid-nitrogen freeze/thaw cycles, prior to Raman–UV DR measurements in a cylindrical glass sample cell at typical sample pressures of 1–5 Torr. The Raman PUMP and STOKES wavelengths used in the experiments are generated by a Nd:YAG/dye laser system (Molectron MY34/DL18P). The pulse duration, energy, and optical bandwidth of the 532 nm (PUMP) radiation are ≈ 15 ns, ≈ 50 mJ, and ≈ 0.07 cm^{-1}, respectively. The corresponding quantities for the tunable 594 nm STOKES radiation are ≈ 12 ns, ≈ 15 mJ, and ≈ 0.3 cm^{-1}, respectively. The tunable UV PROBE radiation is generated by an excimer-pumped dye laser system (Lambda-Physik LPX100/FL3002E with BBO frequency doubler), yielding continuously tunable output in the desired spectral region (240–250 nm) with ≈ 0.3 cm^{-1} optical bandwidth, ≈ 20 ns pulse duration, and ≈ 0.5 mJ pulse energy. All laser beams are linearly polarised in the vertical plane. The two pulsed laser beams generated by the Nd:YAG/dye laser system are overlapped temporally and spatially using a long-wavepass dichroic filter to form the Raman excitation beam (the collinear combination of PUMP and STOKES radiation), and then carefully overlapped with the counterpropagating UV PROBE beam. Two silica lenses of 50 cm focal length are used to focus the Raman excitation and PROBE beams for maximum signal-to-noise ratio. Broadband (300–400 nm) LIF detection of Raman–UV DR signals is achieved with a combination of imaging lens, bandpass filters, and photomultiplier, followed by a suitable preamplifier, boxcar integrator, and data-logging system.

To record figs. 2 and 3, tunable UV PROBE radiation is used to monitor Raman-induced population changes (in the 2_1 and $2_1 4_1$ vibrational levels, respectively) by exciting the 3^1 level in the $\tilde{A}$ electronically excited manifold (using the $2_1^0 3_0^1$ and $2_1^0 3_0^1 4_1^0$ rovibronic bands, respectively), with broadband UV LIF (300–400 nm) monitoring the sequence of pulsed Raman and LIF excitation. In each case, the time delay between the UV PROBE pulse and the Raman excitation pulses (which we call the Raman–UV delay) is minimised, allowing little or no time for collisions during the excitation sequence, so that the re-

sulting spectra are effectively collision-free and characteristic of the directly excited states. Raman–UV DR spectra are usually displayed as difference spectra, with the thermal-equilibrium background signal suppressed to show only the Raman-induced ODR signal.

Increasing the Raman–UV delay enables collision-induced energy transfer processes such as RET [15,17,18] and V–V transfer to intervene. This approach is intrinsic to the experimental scheme represented by fig. 1 and eq. (2). Coherent Raman excitation in the $(\nu_2+\nu_4-\nu_4)$ hot band prepares specific rotational states of the 2_14_1 vibrational level, as may be verified by recording the Raman–UV DR spectrum of the $2_1^0 3_0^1 4_1^0$ rovibronic band as in fig. 2 (but not marked explicitly in fig. 1), with minimal Raman–UV delay. As the Raman–UV delay is increased at a given sample pressure, the collision number z [#6] increases correspondingly and various forms of state-to-state energy transfer arise. One of the most efficient of these processes is expected to be quasi-resonant intermolecular $(2_14_1+0)\rightarrow(2_1+4_1)$ V–V transfer as in fig. 2 and eq. (2), in which a ν_4 vibrational quantum migrates from the initially prepared C_2H_2 molecule to a collision-partner C_2H_2 molecule. This process leaves the state-selected C_2H_2 molecule in the 2_1 vibrational level, which can be monitored by recording the Raman–UV DR spectrum of the $2_1^0 3_0^1 K_0^1$ rovibronic band in the manner of fig. 1. The form of this spectrum is well known [15,17–19], as is shown by the directly excited (collision-free) Raman–UV DR spectrum in fig. 2.

Fig. 4 presents a set of corresponding Raman–UV DR difference spectra arising from the collision-induced process depicted in fig. 1 and eq. (2). The lowest of these spectra, recorded with minimal Raman–UV delay (20 ns) and collision number ($z=1.4$, as determined by the relatively high sample pressure of 4.5 Torr needed for acceptable signal-to-noise ratio), is effectively a null trace. "Subtraction noise," associated with incomplete suppression of intense peaks from the underlying $3_0^1 4_3^0$ band in the thermal-equilibrium background spectrum [15,18], is more prominent than any genuine Raman–UV DR signal in this spectrum; this determines the effective signal-to-noise ratio in these measurements. As the Raman–UV delay (and hence z) increases, the profile of the $2_1^0 3_0^1 K_0^1$ band grows into the Raman–UV DR spec-

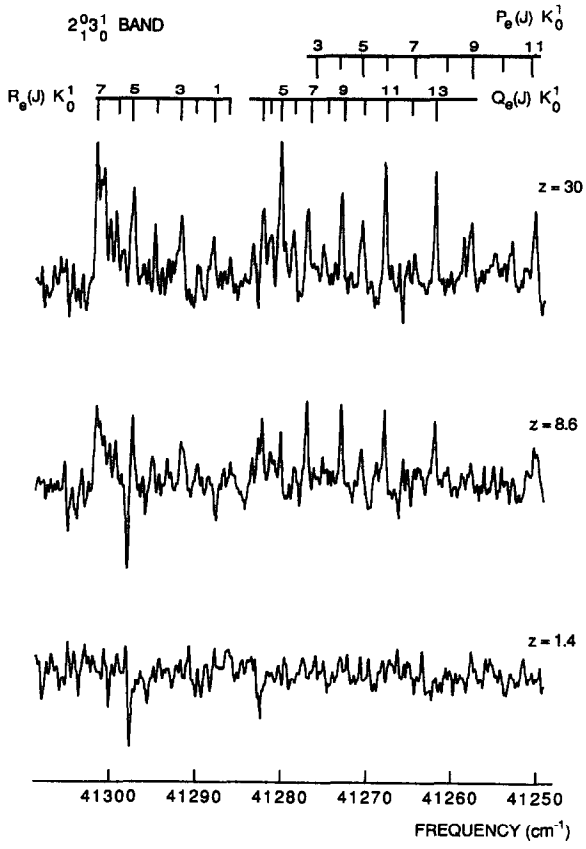

Fig. 4. Raman–UV DR difference spectra in the vicinity of the 242 nm $\tilde{A}\leftarrow\tilde{X}$ $2_1^0 3_0^1 K_0^1$ vibronic band of C_2H_2(g) at 4.5 Torr and 300 K. Coherent Raman excitation (50 mJ at 532 nm and 15 mJ at 594 nm, with Raman bandwidth $\approx$0.3 cm^{-1}) and LIF detection (with UV PROBE bandwidth $\approx$0.4 cm^{-1}) are as in fig. 1. The spectra reveal collision-induced evolution of $(2_14_1+0)\rightarrow(2_1+4_1)$ V–V energy transfer, with three different values of Raman–UV delay t and collision number z (see footnote 6), as follows: lowest trace, $t=20$ ns, $z=1.4_5$; middle trace, $t=120$ ns, $z=8.6_5$; topmost trace, $t=420$ ns, $z=30$. The rotational structure indicated is comparable to that of the same rovibronic band in fig. 2 (which, by contrast, is a directly excited Raman–UV DR spectrum recorded under effectively collision-free conditions with $z=0.16$).

[#6] The collision number z is arbitrarily referenced to a Lennard-Jones rate constant [7,24], $k_{LJ}(C_2H_2/C_2H_2)=16$ μs^{-1} Torr^{-1} $=5.0\times10^{-10}$ cm^3 molecule^{-1} s^{-1} for C_2H_2 self-collisions at 300 K. The same reference point is also used for collisional transfer efficiencies $\mathscr{P}$.

trum. In the topmost trace of fig. 4, with $z=30$, many of the rovibronic features of the $2_1^0 3_0^1 K_0^1$ band (comparable with those in fig. 2) are evident and assignable by the superimposed subband grids.

From the observed rovibronic intensity distributions in fig. 4 (notably the appearance of the R head at $\approx 41\,300\ cm^{-1}$ and the intensity of Q- and P-branch features with $J \geqslant 7$, relative to the narrower spectral distribution of a directly Raman-excited 2_1 level as shown in fig. 2), it is apparent that C_2H_2 molecules appearing in the 2_1 level after $(2_1 4_1+0) \rightarrow (2_1+4_1)$ V–V transfer are rotationally equilibrated. As in the context of figs. 2 and 3, broadband ($\approx 0.3\ cm^{-1}$) Raman excitation was used to prepare a distribution of $2_1 4_1$ (or, in the case of fig. 2, 2_1) rovibrational states with J spanning the range 0–15 [18], far from the thermal-equilibrium distribution. There is no evidence, in the topmost trace of fig. 4, of a "memory" of the initially prepared rotational-state distribution. This is not at all surprising, given that the collision number ($z=30$) is sufficiently high for rotational equilibration by RET to be well established. A variety of Raman–UV DR [15,17,18] and IR–UV DR [20,23,24,26] investigations indicate that the total collision-induced RET efficiency $\mathscr{R}_{RET}$ in C_2H_2/C_2H_2 collisions is in the range 1–2, whereas the efficiency $\mathscr{R}_{V-V}$ of the $(2_1 4_1+0) \rightarrow (2_1+4_1)$ V–V transfer process of interest appears to be smaller by an order of magnitude (as will be confirmed quantitatively in section 3) (see footnote 6). The rotationally resolved V–V transfer studies in this context therefore fall within the "rotationally scrambled" category, as discussed in section 1.

Spectra such as those in fig. 4 provide a qualitative view of the intermolecular V–V transfer process of interest, in which the population of the 2_1 level appears to be reaching a maximum value for $z \approx 20$, but more detailed kinetic experiments are needed to obtain a precise value for the rate of V–V transfer.

3. State-to-state kinetics of $(2_1 4_1+0) \rightarrow (2_1+4_1)$ V–V transfer

The Raman–UV DR experiments described in section 2 generate detailed spectroscopic information concerning direct excitation mechanisms (with minimal Raman–UV delay) and collision-induced energy transfer (with increased Raman–UV delay and collision number z). A second form of ODR experiment entails fixing both the Raman excitation and UV LIF frequencies to identifiable spectroscopic features and continuously varying the Raman–UV delay, to extract kinetic information on the collision-induced population of specific rovibrational quantum states. In the kinetic adaptation of the scheme shown in fig. 1, Raman excitation is centered on the 1961.7 cm^{-1} Q(5) feature of the $(\nu_2+\nu_4-\nu_4)$ hot band [41] while the UV PROBE targets a prominent feature in the 242 nm $2_1^0 3_0^1 K_0^1$ band [15,18]. In the experiments reported, the UV PROBE is held fixed on the $Q_e(5)$ rovibronic feature, predicted [39,41] to be at $41\,280.1_5\ cm^{-1}$ (see figs. 2 and 4). The LIF intensity is then recorded and averaged during successive scans of the Raman–UV delay. The kinetic curves thereby generated register the collision-induced evolution of rovibrational population in the 2_1 level after Raman excitation of the $2_1 4_1$ level, and the rate of intermolecular $(2_1 4_1+0) \rightarrow (2_1+4_1)$ V–V transfer can thence be deduced. The rotationally specific V–V transfer process examined in the state-selected C_2H_2 molecules is therefore that shown in eq. (2) with $J \approx 5$ and $J'=5$, but rotationally scrambled by inevitable RET in both the initial $(2_1 4_1)$ and final (2_1) vibrational levels.

The apparatus and experimental procedures for kinetic measurements are similar to those used in previous IR–UV DR [12,13] and Raman–UV DR [16,18] experiments. Timing of Raman-excitation and UV PROBE pulses is controlled by a digital delay generator (Stanford Research Systems model DG535), with a counter (Hewlett Packard model 5238A) used [13] to measure the Raman–UV DR delay directly. The counter output actively assigns the corresponding instantaneous LIF signal amplitude (for a single sequence of laser pulses) to one of the 512 channels in the microcomputer data-logger used to maintain a running average of the Raman–UV DR signal amplitude during successive sweeps of the delay. The counter imposes an instrumental temporal resolution of ± 10 ns.

Fig. 5 shows a set of Raman–UV DR kinetic curves for $(2_1 4_1+0) \rightarrow (2_1+4_1)$ V–V transfer at three different sample pressures. Experimental data points (averaged during successive time-delay sweeps) are indicated by dots at a particular Raman–UV delay t,

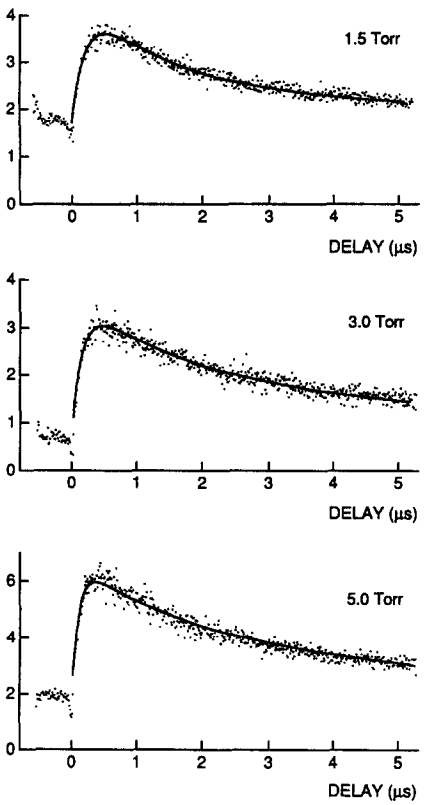

Fig. 5. Kinetic curves demonstrating the growth and decay of the intensity $I(t)$ of the 41280.15 cm^{-1} $Q_e(5)$ feature in Raman–UV DR spectra of the $2_1^0 3_0^1 K_0^1$ vibronic band of $C_2H_2(g)$ at 300 K. Experimental conditions are comparable to those in fig. 4 (recorded by scanning the UV PROBE wavelength with the fixed values of Raman–UV delay t and collision number z), except that the UV PROBE wavelength is now fixed while t (and hence z) is scanned continuously. For the three different sample pressures P (1.5, 3.0, and 5.0 Torr as indicated), the maximum value of $t=5.0$ μs corresponds to values of the collision number $z=120$, 240, and 400, respectively (see footnote 6). Each set of experimental data is digitally recorded with a superimposed curve of best fit, of the form defined in eq. (3) and discussed in the text.

and the solid line represents the least-squares fit of the Raman–UV DR signal intensity $I(t)$ to a fitting function of the form

$$I(t)=A+(1+\beta t/P)^{-1}B \times[\exp(-t/\tau_s)-\exp(-t/\tau_f)]\,, \qquad (3)$$

the time dependence of which is consistent with a simple consecutive kinetic process, with an accompanying mass-transfer loss mechanism (represented by the factor containing β). An additional constant A represents the (relatively high) level of background light detected in the experiment.

The "fast" time constant τ_f in eq. (3) is expected to correlate with the $(2_14_1+0)\rightarrow(2_1+4_1)$ V–V transfer process of interest and the "slow" time constant τ_s represents less efficient collision-induced processes (V–V and V–T, R) deactivating the 2_1 level, each with amplitude factor B. In fitting the Raman–UV DR data over a range of sample pressures P, the value of $(P\tau_s)^{-1}$ is constrained at a value of 0.02 μs^{-1} $Torr^{-1}$ ($\mathscr{P}=1.25\times10^{-3}$), consistent with the range of observed (ultrasonic dispersion and IRF) values [34] for the V–T, R rate constant in $C_2H_2(g)$.

The factor $(1+\beta t/P)^{-1}$ in eq. (3) allows for the effect of diffusion losses on the Raman–UV DR signal intensity. This phenomenon arises from the fact that some laser-excited molecules migrate from the relatively small LIF viewing zone before being probed, thereby introducing a loss mechanism which is not physically significant as far as molecular energy transfer is concerned. The sample pressures ($\geqslant 1$ Torr) and rise-times ($\geqslant 0.1$ μs) encountered are sufficiently large that the dominant mass-transport loss mechanism is diffusion out of the viewing zone, rather than free flight (as occurs in the limit of low pressure and large mean free path). A similar situation has been analysed in the context of laser photolysis experiments [43], showing that diffusion losses from a cylindrical irradiation zone are described by the above correction factor with a parameter β of form

$$\beta=4\mathscr{D}P/(R^2+L^2)\,, \qquad (4)$$

where $\mathscr{D}$ is the self-diffusion coefficient and R and L are the effective diameters of the excitation and probe beams, respectively. Corrections for diffusive losses have been found necessary in other experimental investigations [32,43]. In the limit of low pressures and fast rise-times, the "beam flyout" correction factor takes on a different functional form, as has been recognised in our Raman–UV DR and IR–UV DR studies of RET [16], as well as in other laboratories [24,43,44].

The value of the parameter β in eq. (3) is determined by noting that, on physical grounds, Stern–Volmer plots of τ_f^{-1} against P (such as those in fig. 6) are expected to be linear with zero intercepts. The

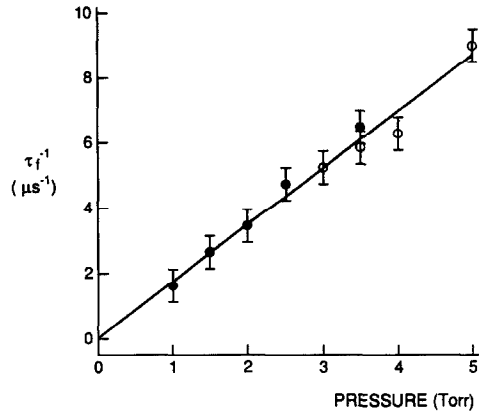

Fig. 6. Plots against C_2H_2(g) sample pressure P of the inverse time constant τ_f^{-1}, obtained by fitting kinetic curves such as those of fig. 5 to eq. (3) as explained in the text. Two separate sets of experimental data (with slightly different Raman-excitation focal geometries) are represented, with vertical bars denoting their uncertainty. The values of the mass-transfer parameter β in the two sets of fitted data are 2.5 μs^{-1} Torr (●) and 1.4 μs^{-1} Torr (○), corresponding to effective focal diameters $(R^2+L^2)^{1/2}$ of 0.12_5 and 0.17 mm, respectively. From the Stern–Volmer law, the slope of the straight line of best fit (common to both sets of data) yields the second-order rate constant $k_{V-V}=1.7_5\pm0.3$ μs^{-1} $Torr^{-1}$, which in turn corresponds to a collisional transfer efficiency $\mathscr{P}_{V-V}=0.11\pm0.02$ (see footnote 6).

beam irradiation parameter (R^2+L^2) in eq. (4) has been treated as an adjustable fitting parameter to match this expectation. The self-diffusion coefficient $\mathscr{D}$ is predicted [7] on the basis of a Lennard-Jones intermolecular potential, defined by the customary collision diameter $d=4.22$ Å and well-depth $\epsilon/k_B=185$ K, using the formula

$$\mathscr{D}=3(N_A k_B^3 T^3/\pi M)^{1/2}[8Pd^2\Omega^{(1,1)*}(T^*)]^{-1}, \quad (5)$$

where M is the molar mass, T^* the reduced temperature $(=k_BT/\epsilon)$, and $\Omega^{(1,1)*}(T^*)$ a characteristic transport coefficient integral [7]. For C_2H_2(g) at 300 K and $P=1$ Torr, $\mathscr{D}$ is estimated to be 9800 $mm^2\,s^{-1}$. Eq. (5) shows that $\mathscr{D}$ is inversely proportional to P, so that eq. (4) ensures that the parameter β is pressure-independent. In two separate sets of experiments with distinct Raman–UV irradiation geometries, the fitting procedure yielded β-values of 2.5 and 1.4 μs^{-1} Torr, respectively. With values of $\mathscr{D}$ predicted by means of eq. (5), the corresponding mean values of $(R^2+L^2)^{1/2}$ are found to be 0.12_5 and 0.17 mm, respectively. These are plausible as effective diameters for the focused, overlapping laser beams in our Raman–UV DR detection zone.

With three of the parameters in eq. (3) – A, β, and τ_s – constrained by inspection as described above, two free-ranging parameters – B and τ_f – remain available to fit the kinetic curves $I(t)$ at various pressures P, as in fig. 5. The time constant τ_f is of prime consideration, since its pressure dependence enables us to evaluate the second-order rate constant k_{V-V} for V–V transfer, by the Stern–Volmer method. The two sets of diffusion-corrected kinetic data are plotted together in fig. 6, showing an acceptable linearity and a common slope corresponding to a macroscopic second-order rate constant (see footnote 3) of $k_f=1.7_3\pm0.3$ μs^{-1} $Torr^{-1}$.

To reduce this result to a microscopic rate constant (see footnote 3) for V–V transfer as in eq. (4), we refer to a simple kinetic model (adapted from that described on pp. 65–67 of ref. [2]). This predicts that the state-to-state microscopic rate constant for collision-induced $(2_14_1+0)\rightarrow(2_1+4_1)$ V–V transfer in the forward direction is smaller than the corresponding macroscopic rate constant, according to the formula: $0.90(k_f-k_s)$, where $k_s=(P\tau_s)^{-1}$ and the numerical factor differs from 1.00 by (small) allowances for detailed-balance and reverse-process effects. It follows, therefore, that $k_{V-V}=1.5_4\pm0.3$ μs^{-1} $Torr^{-1}$, corresponding to a collisional efficiency $\mathscr{P}_{V-V}=0.09_6\pm0.02$ (see footnote 6). This model-based procedure has the effect of reducing the macroscopic rate constant extracted directly from fig. 6. The same model identified the second-order decay rate constant k_s as the weighted-mean rate constant for V–T, R from the 2_14_1 and 2_1 vibrational states (weighted in the ratio 1:9, in accord with the forward and reverse pseudo-first-order rate constants). This is consistent with the value of 0.02 μs^{-1} $Torr^{-1}$ adopted above for $(P\tau_s)^{-1}$ [34]. Further implications of these results, in relation to other studies of vibrational energy transfer in acetylene, will be considered in section 4.

4. Discussion and conclusions

The results of time-resolved Raman–UV DR experiments reported in this paper add to the body of

information on intermolecular V–V transfer in acetylene gas. These are summarised in table 1, and compared with earlier experiments. Numerous additional experimental results on intramolecular V–V transfer [21,25,30, 32, 37] [#7] as well as V–T, R relaxation [21,30,32,33], in acetylene are not covered by table 1.

Our results complement a range of previous experimental investigations of intermolecular V–V transfer in acetylene, based on IRF [30–32] and IR–UV DR [21,23,37,38] techniques. Theoretical [36] and experimental [32,34] studies by Smith and co-workers have scrutinised and, in several respects, re-assessed earlier IRF experiments [30,31] and calculations [33,35]. A contentious issue has entailed identifying a variety of V–V transfer processes, in some cases quasi-elastic, which now appear to contribute to rate constants for vibrational relaxation; these had originally been attributed simply to V–T, R processes. The general principles of vibrational energy transfer have long been established [1–4,6], but there are still several cautionary messages to be noted in this context.

[#7] In collision-induced *intra*molecular V–V transfer, the vibrational energy remains localised in the state-selected molecule, as exemplified by eq. (1), whereas its *inter*molecular counterpart enables vibrational energy to migrate from the state-selected molecule to its collision partner, as in eq. (2) [2].

The first message is obvious from the above comments: that it is not necessarily straightforward to assign rate constants measured in kinetic experiments, whether they be associated with chemical reactions or with physical processes such as energy transfer. Observed rate constants are frequently amenable to misleading mechanistic identification, as is apparent from several instances in the literature of vibrational energy transfer [3]. As a corollary, it follows that more elaborate, species- or state-specific experiments (such as ODR) offer fewer opportunities for misinterpretation than less finely resolved experiments (such as IRF, PAS, ultrasonic dispersion, or thermal lensing). While traditional vibrational relaxation methods [1–4,6,33] can still be informative, their lack of state-specificity can lead to dubious interpretations. The need [32,34,36] to reanalyse early vibrational relaxation data for acetylene [30,33] is a case in point.

Secondly, it must be recognised that, even if a macroscopic rate constant is qualitatively assigned, it is often difficult to extract and quantify the corresponding microscopic rate constant on which any thorough mechanistic interpretation is based (see footnote 3). In this regard, more than one form of experiment (e.g. IRF and ODR) bearing on a common energy transfer channel can help to minimise mechanistic ambiguity. There is no shortage of pub-

Table 1
Measured second-order rate constants k and collisional efficiencies $\mathscr{P}$ for collision-induced intermolecular V–V energy transfer in acetylene (C_2H_2 and C_2D_2) at 300 K

Molecules involved	Energy transfer mechanism [a]	Rate constant k (μs^{-1} Torr^{-1}) [b]	Efficiency $\mathscr{P}$ [c]	Method and references
C_2H_2/C_2H_2	$2_1+0\rightarrow 4_1+4_15_1,\ldots$ [d]	0.021	0.0013	IR fluorescence [30]
C_2H_2/C_2H_2	$3_1/2_14_15_1+0\rightarrow 2_14_1+5_1,\ldots$	$2.4\pm0.1_5$	0.15 ± 0.01	IR fluorescence [32]
C_2D_2/C_2D_2	$4_15_1+0\rightarrow 4_1+5_1$	*$0.4_7\pm0.2_3$*	*$0.02_9\pm0.01_4$*	IR–UV DR [21]
C_2H_2/C_2H_2	$2_14_1+0\rightarrow 2_1+4_1$	*$1.5_4\pm0.3$*	*$0.09_6\pm0.02$*	Raman–UV DR [e]
C_2H_2/C_2H_2	$2_14_1+0\rightarrow 2_1+4_1$	0.8 ± 0.2	0.05 ± 0.01	IR–UV DR [38]

[a] Intermolecular V–V transfer processes are listed in the "shorthand" defined in the context of eq. (2).

[b] Second-order rate constants k are listed in units of μs^{-1} Torr^{-1} (for an ideal gas at 300 K, 1.00 μs^{-1} Torr^{-1} = $3.10_5\times10^{-11}$ cm^3 molecule^{-1} s^{-1}). Microscopic rate constants, which have been obtained by fitting to an appropriate kinetic model, are shown as *italicised* entries. Other rate constants are understood to be macroscopic (phenomenological) rate constants (see footnote 3). For quasi-elastic V–V processes, these tend to be larger (often by a substantial factor) than the corresponding microscopic rate constant; see text for further discussion.

[c] Collisional efficiencies $\mathscr{P}$ are referred to the appropriate Lennard-Jones rate constant [7] (see footnote 6).

[d] The experimental results of ref. [30] have subsequently been re-interpreted in ref. [36]. See also refs. [32,34,35].

[e] This work; see section 3.

lished instances of measured (macroscopic) rate constants being identified as those for particular V–V transfer processes, with the false implication that they are numerically equal to particular microscopic rate constants appearing in the energy-transfer mechanism. Some mechanistic ambiguity can be avoided in cases [25] where it is possible to conduct V–V transfer measurements under single-collision conditions, but this is not always experimentally feasible.

An effort has been made, both in this paper and in our earlier study of V–V transfer in C_2D_2 [21], to construct plausible kinetic models to show the relationship between macroscopic and microscopic rate constants (see footnote 3), and thereby evaluate the latter within experimental error. These microscopic rate constants are italicised in table 1, to distinguish them from macroscopic results from other sources, in which a corresponding model-based transformation has not been performed. There is now a variety of kinetic data for quasi-elastic intermolecular V–V transfer processes of the general from

$$C_2H_2([V]4_1; J, l=1) + C_2H_2(v=0; \tilde{J}, l=0)$$
$$\rightarrow C_2H_2([V]; J', l=0) + C_2H_2(4_1; \tilde{J}', l=1)\,, \quad (6a)$$
$$\rightarrow C_2H_2([V]; \tilde{J}', l=0) + C_2H_2(4_1; J', l=1)\,, \quad (6b)$$

where the symbol [V] denotes a combination of vibrational quanta. For example, the substitution $[V]=2_1$ yields eq. (2), as studied in this paper. Equally applicable equations occur if C_2D_2 is interchanged with C_2H_2, or 5_1 with 4_1. Other cases represented in table 1 include $[V]=4_15_1$ (either member of the $3_1/2_14_15_1$ Fermi dyad of C_2H_2) [32], another study of $[V]=2_1$ as in eq. (2) [38], and $[V]=5_1$ for C_2D_2 [21]. Estimates of the microscopic second-order rate constants k_{V-V} for such processes fall in the range 0.5–1.5 μs^{-1} $Torr^{-1}$, corresponding to a (microscopic) collisional efficiency $\mathscr{P}_{V-V}$ of 0.03–0.10. The efficiency for the first intermolecular V–V transfer process listed in table 1, based on IRF measurements [30] re-assigned in ref. [36], is even smaller; this is presumably because more vibrational quanta need to be concerted in a $(2_1+0)\rightarrow(4_1+4_15_1)$ process, than in $([V]4_1+0)\rightarrow([V]+4_1)$ as in eq. (6).

The rotationally resolved ODR approach to investigations of vibrational energy transfer has several advantages, as already outlined in section 1. These are evident in the present study of intermolecular V–V transfer in C_2H_2 and in our previous work on C_2D_2 [21], not only with respect to experimental sensitivity and specificity but also in terms of the level of mechanistic detail provided. None of the ODR experiments on acetylene, in the present work or in other laboratories [23,25,37,38], are completely free of the scrambling effects of fast RET processes, so that the vibrational transfer rates measured are generally rotationally averaged quantities. This problem may be relieved, and kinetic analysis simplified, if kinetic experiments are performed under single-collision conditions [25], but this usually provides only a partial solution. Nevertheless, there is much useful spectroscopic and kinetic information available from rotationally resolved Raman–UV DR and IR–UV DR experiments. For example, the capability of IR–UV DR to examine specifically prepared rovibrational states is essential in rotationally resolved studies of intramolecular V–V transfer within the $3_1/2_14_15_1$ [37] and $3_3/1_12_13_14_2$ [25] Fermi dyads of C_2H_2. In each case, it appears that V–V transfer from one Fermi-dyad component to another occurs through a wide range of rotationally specific channels, with appreciable efficiencies for values of $|\Delta J|$ as larger as 18. Our complementary Raman–UV DR studies of $(2_14_1+0)\rightarrow(2_1+4_1)$ intermolecular V–V transfer in C_2H_2/C_2H_2 collisions are similarly reliant on state-specific pumping and probing of the rovibrational states involved. Rotational resolution is also a vital feature of our previous experiments [21] on collision-induced V–V transfer involving the $4_2/4_15_1/5_2$ manifold of C_2D_2. This approach is indispensable in resolving the detailed kinetics of simultaneous, competing state-to-state vibrational energy transfer channels and in providing a (relatively rare) means of measuring the absolute amplitude, as well as the timescale, of collision-induced energy transfer.

Our Raman–UV DR and IR–UV DR [21] experiments on vibrational energy transfer in acetylene should be viewed alongside numerous other ODR studies of the same molecule, yielding fundamental spectroscopic information [18,19,27,29] as well as measuring RET processes in both discrete vibrational levels [16–18] and congested manifolds [20,23–26,28]. In cases where the density of rovibrational states is very high, there is much interest in

the interplay of collision-induced RET with underlying intramolecular vibrational redistribution. Our ongoing research includes IR–UV DR experiments involving $(\nu_2+3\nu_3)$-band rovibrational state preparation of C_2H_2 [28], as well as LIF-detected Raman–UV DR and IR–UV DR studies of energy disposal in the photopredissociation of van der Waals molecules of the form C_2H_2–M, where M = Ar, H_2, ... [45].

Acknowledgement

This research was supported by the Australian Research Council, by a Macquarie University Postgraduate Scholarship (to BLC) and by an Australian Postgraduate Research Award (to APM). The work was performed within the Macquarie University Centre for Lasers and Applications. We gratefully acknowledge helpful communications with F.F. Crim, M.J. Frost and I.W.M. Smith (who also provided some particularly constructive criticisms of the draft manuscript).

References

[1] C.B. Moore, Advan. Chem. Phys. 23 (1973) 41;
E. Weitz and G. Flynn, Ann. Rev. Phys. Chem. 25 (1974) 275;
J.D. Lambert, Vibrational and rotational relaxation in gases (Clarendon Press, Oxford, 1977);
R.T. Bailey and F.R. Cruickshank, Chemical Society Specialist Periodical Report, Vol. 3. Gas kinetics and energy transfer (Chem. Soc., London, 1978) pp. 109–199;
R.T. Bailey and F.R. Cruickshank, Advan. Infrared Raman Spectry. 18 (1981) 52;
E.Weitz and G. Flynn, Advan. Chem. Phys. 47 (1981) 185;
J.W. Rich, Appl. At. Collision Phys. 3 (1982) 99;
R.J. Gordon, Comments At. Mol. Phys. 21 (1988) 123;
R.E. Weston and G.W. Flynn, Ann. Rev. Phys. Chem. 43 (1992) 559.

[2] J.T. Yardley, Introduction to molecular energy transfer (Academic Press, New York, 1980).

[3] B.J. Orr and I.W.M. Smith, J. Phys. Chem. 91 (1987) 6106.

[4] B.J. Orr, in: Advances in chemical kinetics and dynamics, Vol. 2. Vibrational energy transfer involving large and small molecules, ed. J.R. Barker (JAI Press, 1993), in press.

[5] J.I. Steinfeld and P.L. Houston, in: Laser and coherence spectroscopy, ed. J.I. Steinfeld (Plenum Press, New York, 1978) pp. 1–123.

[6] R.T. Bailey and F.R. Cruickshank, Chemical Society Specialist Periodical Report, Vol. 2. Molecular spectroscopy (Chem. Soc., London, 1974) pp. 262–356.

[7] J.O. Hirschfelder, C.F. Curtiss and R.B. Bird, Molecular theory of gases and liquids (Wiley, New York, 1954).

[8] F. Ménard-Bourcin and L. Doyennette, J. Chem. Phys. 88 (1988) 5506;
L. Doyennette and F. Ménard-Bourcin, J. Chem. Phys. 89 (1988) 5578.

[9] B. Foy, J. Hetzler, G. Millot and J.I. Steinfeld, J. Chem. Phys. 88 (1988) 6838;
J. Hetzler, G. Millot and J.I. Steinfeld, J. Chem. Phys. 90 (1989) 5434;
J.R. Hetzler and J.I. Steinfeld, J. Chem. Phys. 92 (1990) 7135;
J.I. Steinfeld, in: Advances in chemical kinetics and dynamics, Vol. 2. Vibrational energy transfer involving large and small molecules, ed. J.R. Barker (JAI Press, 1993), in press.

[10] B.J. Orr, Intern. Rev. Phys. Chem. 9 (1990) 67.

[11] J.G. Haub and B.J. Orr, J. Chem. Phys. 86 (1987) 3380.

[12] C.P. Bewick and B.J. Orr, J. Chem. Phys. 93 (1990) 8634;
C.P. Bewick, J.F. Martins and B.J. Orr, J. Chem. Phys. 93 (1990) 8643.

[13] C.P. Bewick, J.G. Haub, R.G. Hynes, J.F. Martins and B.J. Orr, J. Chem. Phys. 88 (1988) 6350.

[14] C.P. Bewick, A.B. Duval and B.J. Orr, J. Chem. Phys. 82 (1985) 3470;
C.P. Bewick and B.J. Orr, Chem. Phys. Letters 159 (1989) 73.

[15] B.L. Chadwick, D.A. King, L. Berzins and B.J. Orr, J. Chem. Phys. 91 (1989) 7994.

[16] B.L. Chadwick, Ph.D. Thesis, Macquarie University (1991).

[17] R. Dopheide, W.B. Gao and H. Zacharias, Chem. Phys. Letters 182 (1991) 21.

[18] B.L. Chadwick and B.J. Orr, J. Chem. Phys. 97 (1992) 3007.

[19] H.-D. Barth, A.P. Milce, B.L. Chadwick and B.J. Orr, J. Chem. Soc. Faraday Trans. 88 (1992) 2563.

[20] E. Carrasquillo M., A.L. Utz and F.F. Crim, J. Chem. Phys. 88 (1988) 5976.

[21] B.L. Chadwick and B.J. Orr, J. Chem. Phys. 95 (1991) 5476.

[22] A.L. Utz, Ph.D. Thesis, University of Wisconsin – Madison (1991).

[23] M.J. Frost and I.W.M. Smith, Chem. Phys. Letters 191 (1992) 574.

[24] A.L. Utz, J.D. Tobiason, E. Carrasquillo M., M.D. Fritz and F.F. Crim, J. Chem. Phys. 97 (1992) 389.

[25] J.D. Tobiason, Ph.D. Thesis, University of Wisconsin – Madison (1992);
J.D. Tobiason, A.L. Utz and F.F. Crim, in: Laser techniques for state-selective and state-to-state chemistry (Proceedings of SPIE Conference 1858, January 1993).

[26] J.D. Tobiason, A.L. Utz and F.F. Crim, J. Chem. Phys. 97 (1992) 7437.

[27] A.L. Utz, J.D. Tobiason, E. Carrasquillo M., L.J. Sanders and F.F. Crim, J. Chem. Phys. 98 (1993) 2742;
J.D. Tobiason, A.L. Utz and F.F. Crim, J. Chem. Phys. (1993), in press.

[28] A.P. Milce, H.-D. Barth, B.L. Chadwick and B.J. Orr, in: High resolution spectroscopy, Technical Digest of OSA Topical Meeting, Salt Lake City, UT, 18–21 January 1993 (Optical Society of America, Washington, DC, 1993) pp. 8,9;
A.P. Milce, H.-D. Barth, B.L. Chadwick and B.J. Orr, unpublished results (1993).
[29] Y. Chen, S. Halle, D.M. Jonas, J.L. Kinsey and R.W. Field, J. Opt. Soc. Am. B 7 (1990) 1805;
K. Yamanouchi, N. Ikeda, S. Tsychiya, D.M. Jonas, J.K. Lundberg, G.W. Adamson and R.W. Field, J. Chem. Phys. 95 (1991) 6330.
[30] J. Häger, W. Krieger, T. Rüegg and H. Walther, J. Chem. Phys. 72 (1980) 4286.
[31] J. Häger, W. Krieger and J. Pfab, J. Chem. Soc. Faraday Trans. II 77 (1981) 469.
[32] I.W.M. Smith and J.F. Warr, Chem. Phys. Letters 173 (1990) 70.
[33] J.L. Stretton, J. Chem. Soc. Faraday Trans. 61 (1965) 1053.
[34] N.J.G. Smith, C.C. Davis and I.W.M. Smith, J. Chem. Soc. Faraday Trans. II 81 (1985) 417.
[35] S.F. Fischer and A. Irgens-Defregger, J. Phys. Chem. 87 (1983) 2054.
[36] A. Miklavc and I.W.M. Smith, J. Chem. Soc. Faraday Trans II 84 (1988) 227.
[37] M.J. Frost, J. Chem. Phys. (1993), in press.
[38] M.J. Frost and I.W.M. Smith, private communication (1993).
[39] J.K.G. Watson, M. Herman, J.C. Van Craen and R. Colin, J. Mol. Spectry. 95 (1982) 101.
[40] J.M. Brown, J.T. Hougen, K.-P. Huber, J.W.C. Johns, I. Kopp, H. Lefebvre-Brion, A.J. Merer, D.A. Ramsay, J. Rostas and R.N. Zare, J. Mol. Spectry. 55 (1975) 500.
[41] E. Kostyk and H.L. Welsh, Can. J. Phys. 58 (1978) 534;
I.-Y. Wang and A. Weber, Ind. J. Phys. 16 (1978) 358.
[42] J. Pliva, J. Mol. Spectry. 44 (1972) 145.
[43] S.E. Bialkowski, D.S. King and J.C. Stephenson, J. Chem. Phys. 72 (1980) 1156.
[44] J.C. Stephenson and D.S. King, J. Chem. Phys. 69 (1978) 1485.
[45] D.E. Heard, A.P. Milce, R.E. Miller and B.J. Orr, unpublished results (1993).